Magnetoacoustic Phenomena In MHD Generators

Author(s): A. Currie Munce, Jr., M. Mitchner, and J. K. Koester

Session Name: Generators

SEAM: 22 (1984)

SEAM EDX URL: https://edx.netl.doe.gov/dataset/seam-22

EDX Paper ID: 1038

MAGNETOACOUSTIC PHENOMENA IN MHD GENERATORS

A. Currie Munce, Jr., M. Mitchner and J. K. Koester†

High Temperature Gasdynamics Laboratory
Stanford University, Stanford, California

ABSTRACT

The solutions of an MHD dispersion relationship have been examined to analyze the magnetogasdynamic effects on the acoustic and entropy waves in an MHD generator, with emphasis on both the magnetoacoustic phase velocities, and wave amplitudes. The analysis was facilitated by the introduction of a new nondimensional frequency which incorporates the effects of frequency and the magnetic interaction parameter in one variable. To measure the relatively small effects predicted for laboratory-scale MHD generators, special experimental methods were developed, based on the use of a low frequency acoustic excitation and the analysis of the phase difference between pressure signals measured at different locations in the MHD generator. Preliminary results from experiments performed using the Stanford M-2 MHD generator facility demonstrate good agreement between the experimental data and solutions of the MHD dispersion relationship.

INTRODUCTION

Fluctuations and nonuniformities are inherent in combustion-driven MHD generators. These fluctuations and nonuniformities may result, for example, from combustor generated noise, nonuniform mixing in the combustion process, and turbulent fluctuations in the flow field. These inherent fluctuations can be measured as fluctuations in the plasma pressure, temperature, density, and velocity. The fluctuating quantities may be viewed as consisting of two parts, wave-like disturbances, and background noise. The wave-like disturbances are of two types; upstream- and downstream-traveling magnetoacoustic waves, and a magnetoentropic wave that travels with a speed approximately equal to that of the gas. The wave-like part demonstrates a strong propagational character, while the noise portion tends to be dissipative with only a weak propagational character. The magnetoacoustic fluctuations are of particular interest because they involve a transport of energy which can experience a significant magnetoacoustic interaction while propagating back and forth through an MHD generator.

Fluctuations are important in MHD generators because of the strong dependence of the electrical conductivity and Hall parameter on the flow condi-

† Advanced Technology Consultant

tions. Relatively small fluctuations in the plasma temperature and pressure, for instance, can induce large nonuniformities in the plasma electrical conductivity. This dependence of the plasma properties on the wave-type disturbances provides a mechanism through which energy in the wave modes can be coupled, by means of the external circuitry, to the energy in the high enthalpy gas. Fluctuations in fluid properties serve as sources of acoustic-like disturbances which in turn, via the electric circuits, generate further fluctuations. The existence of such a mechanism for the exchange of acoustic and electrical energy and hence the possibility of large propagating fluctuations was first described in some early work [1-3] on magnetoacoustic interactions. Later work [4-7] suggested that for certain operating conditions this mechanism could lead to instabilites in MHD generators.

Whether instabilities develop or not, the coupling between the inherent fluctuations in an MHD generator and the electrical power circuitry is undesirable and can affect an MHD generator's performance in many different ways. Even moderate acoustic oscillations could produce large plasma nonuniformities, which would lead to degradation of an MHD generator's electrical performance. Interactions and oscillations may develop between the magnetoacoustic field and the electrical load circuitry which would affect the development of advanced power conditioning circuits. This type of interaction may already have been observed at the CDIF facility during tests of the inverter circuits [8]. The understanding of the nature of the magnetoacoustic interaction is important for the future design and success of large-scale MHD power plants.

The most common method of studying the nature of the magnetoacoustic interaction analytically (and thereby obtaining predictions of wave growth or attenuation, and phase velocity, etc.) has been to examine the solutions of an MHD dispersion relationship. Experimental data are needed in order to assess the validity of the analytical model and the approximations used in deriving this MHD dispersion relationship. No experimental results to date have been reported that enable a comparison to be made with solutions of the MHD dispersion relationship. The reason for this state-of-affairs is that, in small interaction, laboratory-scale MHD generators, the predicted magnetoacoustic effects are small and often overwhelmed by competing effects [9,10]. To attempt to measure predicted magnetoacoustic effects, well-designed experiments with sensitive measurement techniques are needed. This paper will present the results of a series of experiments performed using the Stanford M-2 facility which clearly demonstrate the magnetoacoustic effects on the two acoustic-like waves in a MHD generator. These data can be used to assess certain aspects of the magnetoacoustic theory.

THEORETICAL DEVELOPMENT

Dispersion Relationship

The theoretical approach involves the solution of essentially the same MHD dispersion relationship as described by Barton [7]. It comes from a first-order linearization of the three quasi-one dimensional MHD conservation equations for time dependent perturbations about a known steady-state solution. The linearization is done in terms of the acoustic variables, p', u', T', pressure, velocity and temperature, respectively, and includes variations in

plasma properties such as electrical conductivity and chemical composition. The MHD channel is modeled as a forced boundary value problem in which all disturbances are only allowed to originate either at the upstream or downstream boundaries. The linearity of this system of equations requires that fluctuations in the MHD channel always be of the same frequency as the boundary excitation source. For this reason traveling wave solutions of the form $\exp\{i(kx-\omega t)\}$ may be assumed to satisfy the equations. The result is a cubic dispersion relationship whose roots yields three complex wave numbers, $k = k_r + ik_i$, which are functions of the angular frequency ω and of the MHD interaction parameter S. These three complex wave numbers represent three different types of waves; a downstream magnetoacoustic, an upstream magnetoacoustic, and a convected magnetoentropic wave. The imaginary part of the complex wave number describes the magnetoacoustic effect on the amplitude of the three waves because the amplitude is proportional to $\exp(-k_i x)$. The real part of the complex wave number describes the magnetoacoustic effect on the phase velocity of the three waves. The phase velocity is related to the the real part of the wave number , k_r, by $c_{phase} = \omega/k_r$.

For the present theoretical study several approximations have been used in simplifying the MHD dispersion relationship. For the electrical equations an ideal Faraday generator has been used with infinite segmentation, and the boundary layer voltage drops have been lumped together and included in the external circuits. The effect of steady-state axial property gradients, and viscous and thermal conduction effects have been ignored. No significant change in the nature of the solutions to the dispersion relationship is expected due to the use of these modeling approximations. It may be noted that two and three dimensional models have shown the quasi-one dimensional model (long wavelength model) to be reasonably accurate over a wide range of frequencies [11].

The results from the numerical solution of this MHD dispersion relationship for conditions typical of those that can be obtained in the Stanford M-2 MHD generator facility are shown in Figures 1-3. In these figures both the effect on the phase velocity and the effect on wave amplitude are demonstrated. In these graphs the abscissa is a nondimensional frequency particularly useful for the study of magnetoacoustics. It is expressed in terms of the angular frequency, ω, the length of the duct, L, the isentropic speed of sound, a_o, the magnetic interaction parameter, S, and the Mach number of the flow, M. For conditions typical of those in the Stanford M-2 facility the magnitude of this nondimensional frequency is equal to one when the physical frequency is about 125 Hz.

The first graph of each set represents the MHD effect on the phase velocities of the three waves in an MHD generator. For the case of no MHD interaction, the phase velocities for the two magnetoacoustic waves and the magnetoentropic wave reduce to the well known expressions $c_{phase} = u \pm a_o$ and $c_{phase} = u$ respectively. Here u is the fluid velocity, a_o is the isentropic speed of sound, and the upper and lower signs apply respectively to downstream and upstream-traveling acoustic waves. For the general case, it is convenient to define a wave velocity, a, as the difference between the phase velocity of the wave and the fluid velocity. The MHD effect on the phase velocity of a wave can then be represented by the deviation of a/a_o from one for the two magnetoacoustic waves and the deviations from zero for the magnetoentropic

wave. The dependence of the a/a_o curves on Mach number has been found numerically to be small over a wide range of Mach numbers from 0.15 to 0.80.

In the wave amplitude graphs the imaginary part of the wave number is divided by the product (S•M) to allow all the dependence on the magnetic interaction parameter to be explicitly displayed in these graphs. The fact that the curves are almost constant for sufficiently large values of the nondimensional frequency $\hat{\omega}$ demonstrates that k_i scales linearly with S over a wide range of frequencies and interaction parameters. The effect of changes in Mach number on the values of the wave amplitudes for large $\hat{\omega}$ scales almost directly with residence time in the channel for each of these waves. For instance, for a downstream-traveling wave [phase velocity proportional to (1+M)] the residence time in the channel decreases as the Mach is increased, and the large $\hat{\omega}$ value of the curve decreases proportional to changes in (1+M). The parameter which has the largest effect on both the phase velocity and the wave amplitude curves is the Faraday load factor, K_F.

Solutions of this MHD dispersion relationship (or of similar relations) have been studied extensively [1-7], with particular attention paid to the solution for the imaginary part of the wave number, because the value of k_i governs the possible occurrence of MHD instabilities. The present study has brought out two new interesting features of the solutions which have either previously not been identified or emphasized. The first is the large MHD effect on the phase velocity especially at low frequencies. The magnitude of this effect is demonstrated in Figures 1(a), 2(a), and 3(a). The second (and more important) feature is the introduction of the nondimensional frequency given in Figures 1-3. With the use of this nondimensional frequency, the entire dependence of the solution on frequency and magnetic interaction parameter is displayed explicitly. There is no other implicit dependence on frequency or MHD interaction. This simplication will apply as long as steady-state axial property gradients, and viscous and thermal conduction effects are ignored. The physical reason for this nondimensional grouping is that for acoustic fluctuations the inertial force scales with angular frequency ω. This nondimensional grouping is, then, a ratio of the acoustic inertial force to the MHD $\vec{J}\times\vec{B}$ force. The use of this nondimensional frequency helps to clarify the nature of the MHD interaction, particularly at low frequencies.

Channel Acoustics

The simplest acoustic model for an MHD channel is a constant area duct with an excitation source upstream and a known boundary condition downstream, as shown schematically in Figure 4. The pressure field inside the duct can be described analytically by the simple acoustic wave equation, which requires two boundary conditions, one upstream and one downstream. A useful form in which to specify the downstream boundary condition is in terms of a complex reflection coefficient, R_1. The upstream boundary condition must specify the nature of the upstream excitation source and how it varies in amplitude as a function of frequency.

Under ordinary acoustic conditions the solution to the wave equation yields a pressure field inside the duct that can be expressed as the superposition of a downstream- and an upstream-traveling wave;

$$p'(x,t) = A\, e^{i(k_d x - \omega t)} + B\, e^{-i(k_u x + \omega t)} \quad . \qquad (1)$$

The downstream boundary condition, R_1, can be used to relate the coefficients A and B in this expression by

$$R_1 = r\, e^{i\theta} = \frac{P_{up}}{P_{down}}\bigg|_{x=1} = \frac{B}{A}\, e^{-i(k_u + k_d)\cdot 1} \quad . \qquad (2)$$

Equation (1) can then be rearranged in the form

$$p'(x,t)=Re\{\, A\, e^{-ik_{rd}\cdot 1}\, e^{-k_{id}\cdot x} \sqrt{1 + r'^2 + 2r'\cos[\,2\bar{k}(x-1)+\theta\,]}\; e^{i\phi} e^{i\omega t}\} \qquad (3)$$

where $r' = r\, e^{(k_{iu} + k_{id})\cdot 1}$,

$$\bar{k} = \frac{k_{ru} + k_{rd}}{2} \quad ,$$

and ϕ is the phase angle given by

$$\tan\phi = \frac{r' \sin[\, k_u(x-1) + \theta\,] - \sin[\, k_d(x-1)\,]}{r' \cos[\, k_u(x-1) + \theta\,] + \cos[\, k_d(x-1)\,]} \quad . \qquad (4)$$

The subcripts r and i refer to real and imaginary part, and the subcripts u and d refer to the downstream- and upstream-traveling acoustic-like waves respectively.

The coefficient A in Eq. 3 can be determined once the upstream boundary condition is specified. To determine the phase of the pressure wave in the duct from Eq. 4, A is not needed and hence the upstream boundary condition is not needed. The phase anywhere in the duct is only a function of the downstream reflection boundary condition and is independent of the upstream excitation source. This is particularly advantageous in an MHD generator where the exact nature and amplitude of the upstream source is unknown.

The phase angle as defined in Eq. 4 contains an arbitrary constant. A more unambiguous quantity is the phase difference between two pressure signals measured at different axial locations in the duct. For the idealized case where there are no dissipative losses, R_1=1, and M=0, this quantity depends on frequency as shown in Figure 5. The phase difference is always 0 or 180 degrees with sharp transitions in between. The reason for this behavior can be explained in terms of the envelope of the standing-wave pattern that exists in the duct. For this simple case, the envelope of the pressure fluctuations at a given frequency would look similar to that shown in Figure 6. The downstream boundary is always an antinode if the reflection coefficient is real and positve. The locations of the nodes in this pattern correspond to the minima in the square root term in Eq. 3. In this case

$$\cos[\, 2\bar{k}(x-1) + \theta\,] = -1$$

or $$2\bar{k}(x-1) + \theta = -(2n+1)\pi \qquad n = 0,\pm 1,\pm 2,\ldots$$

and so $(x-1)_{node} = -\frac{(2n+1)\pi + \theta}{2\bar{k}}$. (5)

The first node occurs for n = 0, and successive nodes in the standing-wave pattern correspond to incremental values of n.

The behavior of the phase difference in Figure 5 can be understood by examining the locations of the nodes in Figure 6 relative to the two axial measurement locations. If the two axial locations are separated by an even number of nodes, the phase difference is 0 degrees, and if they are separated by an odd number of nodes, the phase difference is 180 degrees. The transition between 0 and 180 degrees occurs when one of the measurement locations happens to be a node. The location and spacing of the nodes changes when the frequency changes as described by Eq. 5. Starting at low frequencies the nodes are widely spaced, and the two axial locations are not separated by any nodes and hence no phase difference. As the frequency increases, all the nodes move toward the downstream boundary. The frequency at which the location of the first node is equal to that of the most upstream of the two axial locations is the frequency at which the first transition to 180 degrees occurs in Figure 5. Successive transitions occur as nodes, which continue to move closer to the downstream boundary as the frequency increases, pass by one or the other of the measurement locations. For these idealized conditions, measurements of the transition frequencies would enable the sound speed to be determined.

This simple example illustrates the basic principles that underlies the experiments to be described later. Under real conditions, dissipation, mean fluid flow and an imperfectly reflecting downstream boundary produce distortions in the idealized dependence of the phase difference on frequency, but the same basic behavior is preserved. Because of nonideal effects, the transitions are more gradual and the peak values are less than 180 degrees.

Magnetoacoustic Effects on the Phase Difference

For MHD conditions, the character of the dependence of the phase difference on frequency will be influenced by the two effects shown in Figures 1 and 2; namely the MHD effects on the phase velocity and on the damping of the acoustic-like waves. The frequency at which a sharp transition in the phase difference occurs (under idealized conditions) is directly related to the average phase velocity of the two magnetoacoustic waves. The relationship can be seen by rewriting Eq. 5 in terms of the transition frequencies that would be observed at a fixed measurement location;

$$\bar{k}_{trans} = -\frac{(2n+1)\pi + \theta}{2(x-1)} ,$$

and if $$\omega = \bar{k} \cdot \bar{c} ,$$

then $$\omega_{trans} = \bar{c}\,\frac{(2n+1)\pi + \theta}{2(1-x)} .$$

One can see that that any change in $\bar{c}$ will lead directly to a shift in the transition frequency. The shift in frequency would be relatively easy to measure if the transitions in the phase difference plots were sharp. As an example, Figure 7 demonstrates the effect on a phase difference plot of a 5 percent reduction in $\bar{c}$. (In the real case, the reduction in $\bar{c}$ will vary strongly with frequency, and the effect at the second transition would be less

than at the first.) In this figure the shift in frequency caused by the small change in $\bar{c}$ is easily visible. The more gradual the transitions become due to acoustic losses, the less sensitive the technique becomes for measuring changes in the average phase velocity.

Ordinary acoustic effects can cause $\bar{c}$ to change due to variations in the Mach number. The average phase velocity of the two acoustic waves is proportional to $(1-M^2)$. Any increase in the Mach number causes a reduction in $\bar{c}$ and hence causes the transition frequencies to shift to lower values. The effect that a nonzero Mach number can have on the phase difference is demonstrated in Figure 8. The small negative slope in the M = 0.2 curve is due to the fact that the phase velocities of the downstream- and upstream-traveling waves are different when there is a mean gas velocity.

The peak values of the phase difference and the shape of the dependence on frequency in the region of the transitions are sensitive to the amount of acoustic loss there is in the channel. There are two sources of acoustic loss, transmission loss at the exit due to an imperfectly reflecting boundary, and dissipative losses in the flow due to viscous and thermal effects. Transmission loss affects the phase difference because it makes the value of r in Eq. 4 less than one. Figure 9 demonstrates what happens to the phase difference when the value of r is reduced from 1.0 to 0.71 (the experimental value). The dissipative loss affects the phase difference because the exponetial term in the expression for r' becomes less than one if k_i is greater than zero. Figure 10 demonstrates the effect of two different values of k_i on the phase difference. The two values of k_i used in this figure correspond to typical values for (1) normal acoustic dissipative losses, and (2) MHD dissipation losses in the Stanford M-2 channel (see Figures 1b,2b).

In the actual case changes in dissipation and phase velocity caused by MHD effects occur simultaneously. The combined effect for a reduction in $\bar{c}$ of 5 percent is shown in Figure 11 in comparison with the effect of dissipation alone. The 5 percent effect is not nearly as pronounced in this case as it is in Figure 7. Comparing Figures 9 and 10, one can see that if the MHD effects on the phase velocity are 5 percent or less, the changes in the phase difference plots due to the MHD effect on k_i will be more pronounced than those due to the MHD effect on $\bar{c}$. The dissipation effect can also be measured more accurately because it is easier to detect the lowering of the peak level of the phase difference than it is to detect small shifts in the rising edge of the transitions.

Experimental Considerations

The change in the phase difference produced by MHD effects on both the dissipation and the phase velocity will be maximized if the measurements are made at as low a frequency as possible. For the phase velocity it is obvious from Figures 1 and 2 that the largest effects on $\bar{c}$ would be observed at low frequencies. For the dissipation the desirability of low frequencies is not as obvious because the value of k_i from these figures is relatively independent of frequency over the range of frequencies of interest. However the measurement of the magnetoacoustic effect on k_i really involves measuring the incremental magnetoacoustic dissipation in excess of the normal acoustic dissipation, as shown in Figure 9. The classical expression for the amount of normal acoustic dissipation in a tube is [12]

$$k_i = \frac{1}{2a_o}\left(\frac{\omega\nu}{2}\right)^{1/2}\frac{P}{S}\left(1 + \frac{\gamma-1}{\sqrt{Pr}}\right) \qquad (6)$$

where ν is the kinematic viscosity,
P is the perimeter of the duct,
S is the cross sectional area of the duct,
γ is the ratio of specific heats,
and Pr is the Prandtl number of the gas.

The acoustic dissipation scales with the square root of frequency, and hence the relative effect of the magnetoacoustic dissipation with respect to the normal acoustic impedance will be larger for lower frequencies.

Three methods were devised to produce transitions in the phase difference at the lowest possible frequencies. One method involved extending the test section beyond the active MHD channel. Because this arrangement tends to diminish the magnitude of the magnetoacoustic effects in the combined MHD duct and its continuation, the length of the extension must be limited. A second method involved the use of an enlarged cross sectional area for the test section extension. The effect of this area change on lowering the transition frequencies will be discussed in the next subsection. The third approach involved placing a small-area orifice at the downstream end of the test section extension just upstream of the exhaust ducting, and adjusting the flow rate and back pressure so as to achieve choked flow in the orifice. For choked flow through an orifice, the acoustic reflection coefficient is [13]

$$R_{orifice} = \frac{1-\alpha M}{1+\alpha M} \qquad (7)$$

where

$$\alpha = \frac{\left[1+\frac{(\gamma-1)M}{2}^{2}\right]}{\left[1+\frac{(\gamma-1)}{2}\right]} \quad .$$

The use of the choked-flow orifice as the downstream boundary of the test section has three advantages. First, it provides a known, constant downstream boundary condition. Secondly, it decouples the downstream exhaust acoustics (which had plagued preliminary magnetoacoustic experiments [14]) from the MHD channel acoustics. The last and most important property of the orifice is that the reflection coefficient is real and positive and hence approximates an acoustically closed end. The first transition frequency for a closed-end system is one-half that of an open-end system. An open-end system is approximately what would be obtained if the channel were to terminate through a diffuser (or otherwise) into the larger area exhaust ducting. This factor of two can make a significant difference particularly on the measurement of the magnetoacoustic effect on the phase velocity.

Two Region Model

Equations 1-4 describe the acoustics properties of a highly simplied model of a MHD channel in which the duct area is constant and the gas properties are uniform in the axial direction. As described in the preceding subsection, the actual experimental arrangement is better modeled as consisting of two regions; an upstream region in which the waves are magnetoacoustic, and a downstream region in which the waves are (ordinary) acoustic. A schematic of the two-region model is shown in Figure 11. An area change at the interface

between the regions has been included to lower the transition frequencies at which the phase difference changes. (The reason why the area change lowers the frequency of the transitions will be discussed later.)

The dependence of the phase difference on frequency for this two region problem is obtained by employing the known solutions in each region separately, and then applying the matching condition at the interface that the pressure and volume flow rate be continuous. In ordinary acoustics the specific acoustic impedance (ratio p'/u') is $\rho_o a_o$, but in magnetoacoustics this is no longer true. The dispersion relationship must be used to determine the specific acoustic impedance, which may be different for the upstream- and downstream-traveling magnetoacoustic waves. To allow for this variable impedance, the equations are left generalized in terms of a normalized specific impedance

$$z = \frac{p'}{u'} \frac{1}{\rho_o a_o} \quad .$$

In analogy with the one region model, the pressure and velocity fields in region 1 can be written

$$p'_1 = A_1 e^{i(k_{1d}x - \omega t)} + B_1 e^{-i(k_{1u}x + \omega t)} \tag{8a}$$

$$u'_1 = \frac{A_1}{z_{1d}} e^{i(k_{1d}x - \omega t)} + \frac{B_1}{z_{1u}} e^{-i(k_{1u}x + \omega t)} \quad , \tag{8b}$$

and similarly for region 2

$$p'_2 = A_2 e^{i(k_{2d}x - \omega t)} + B_2 e^{-i(k_{2u}x + \omega t)} \tag{9a}$$

$$u'_2 = \frac{A_2}{z_{2d}} e^{i(k_{2d}x - \omega t)} + \frac{B_2}{z_{2u}} e^{-i(k_{2u}x + \omega t)} \quad . \tag{9b}$$

The matching condition at $x=l_1$ is

$$p'_1 = p'_2 \quad \text{and} \quad u'_1 S_1 = u'_2 S_2 \quad . \tag{10}$$

The reflection coefficient at $x=(l_1+l_2)$ can be expressed as

$$R_2 = \frac{B_2}{A_2} e^{-i(k_{2u} + k_{2d})\cdot(l_1+l_2)} \quad . \tag{11}$$

If a reflection coefficient for region 1 is defined as

$$R_1 = \frac{B_1}{A_1} e^{-i(k_{1u} + k_{1d})\cdot l_1} \quad ,$$

then Eq.'s 8-11 can be used to solve for R_1. The result is

$$R_1 = \frac{\left[1 + \tilde{R}_2 \right] - z_{12} S_R \left[1 - z_{2R} \tilde{R}_2 \right]}{z_{1R} \left[1 + \tilde{R}_2 \right] + z_{12} S_R \left[1 - z_{2R} \tilde{R}_2 \right]} \qquad (12)$$

where $\tilde{R}_2 = R_2 e^{i(k_{2u}+k_{2d})\cdot l_2}$,

and $z_{12} = \frac{z_{1d}}{z_{2d}}$, $z_{1R} = -\frac{z_{1d}}{z_{1u}}$, $z_{2R} = -\frac{z_{2d}}{z_{2u}}$, and $S_R = \frac{S_2}{S_1}$.

The solution for the pressure field in region 1 is then given by Eq.'s 3 and 4 if the value for the reflection coefficient given in Eq. 12 is used in place of Eq. 2. When using Eq.'s 3 and 4 in this two region model, the lengths and wave numbers that appear in those equations should be those for region 1 alone. All previous discussions about the nature and character of the phase difference plots still apply to the solutions obtained with this two region model.

The increase in the cross sectional area was included in the two region model because of the effect it can have on reducing the first transition frequency at which the phase difference changes. As an example, Figure 13 demonstrates the relative shift in the transition frequency caused by changing the area ratio S_R from 1.0 to 2.4. The 35 percent decrease in the first transition frequency produces a significant increase in the magnitude of the magnetoacoustic effects on both the change in the damping and the phase velocities.

The decrease in the transition frequency occurs because the matching condition, Eq. 10, requires a discontinuity in u' and the specific acoustic impedance at the interface. The standing-wave envelope, as depicted in Figure 14, will also have a discontinuity at the interface which results in the first node moving closer to the downstream boundary. The change in the standing-wave envelope effectively reduces the wavelength at any given frequency. The shorter wavelengths cause the transition frequencies to shift to lower values.

The analysis for the effect of a sudden area change assumes purely one-dimensional flow. This description is obviously approximate, particularly in the vicinity of the area change. The model can most easily be corrected for two- and three-dimensional effects by using a effective value of S_R in the theory which is somewhat less than the geometrical value. The effective value of S_R can be found by performing a "calibration" measurement of the test section under known conditions. For these experiments, the calibration was done using room temperature nitrogen.

EXPERIMENTAL APPARATUS AND PROCEDURES

Experimental Facility

All experiments were conducted in the Stanford M-2 MHD facility of the High Temperature Gasdynamics Laboratory (HTGL). The flowtrain consisted of a combustor, plenum, nozzle, and run-in section upstream of the active MHD channel region. Downstream of the test section the run-out section had a cross sectional area 2.7 times that of the active MHD region. The run-out was terminated by a choked-flow orifice followed by the scrubbing and exhaust system.

All internal surfaces upstream and including the active MHD region were lined with MgO brick to minimize the heat loss. In the downstream components the internal surfaces were unbricked and made of water cooled copper or stainless steel. A schematic of the Stanford M-2 flowtrain used for these series of magnetoacoustic experiments is shown in Figure 18. Some of the important flowtrain dimensions are listed in Table I.

TABLE I M-2 Flowtrain Dimensions

Combustor	diameter =	9.0 cm	length =	37 cm			
Plenum	width =	9.7 cm	height =	22 cm	length =	38 cm	
Nozzle	inlet width =	6.0 cm	inlet height =	13 cm			
	exit width =	3.0 cm	exit height =	10 cm	length =	5 cm	
Channel	width =	3.0 cm	height =	10 cm	length =	108 cm	
Run-out	width =	6.6 cm	height =	13 cm	length =	51 cm	
Orifice	width =	1.4 cm	height =	6.8 cm			
Magnet	active length = 50 cm						

Spacing between Microphones in the MHD Channel : 21.9 cm
Distance from Downstream Microphone #3 to MHD Channel Exit : 17.1 cm

The experiments were all performed with the MHD generator operating in a normal, segmented Faraday configuration with thirteen electrode pairs. Banks of lead-acid batteries could be inserted into the individual external load circuits in increments of 120 V to augment the current density to values in excess of 1.0 A/cm^2. The MHD plasma was produced by near stoichiometric combustion of ethanol and oxygen. Potassium hydroxide was mixed with the ethanol to produce about 2% Potassium by weight in the products, which produced an electrical conductivity with a nominal value of 15 mhos/m. The static pressure in the channel was nearly atmospheric with a nominal core temperature of 2750 K. The Mach number of the plasma was kept low, near 0.20, to maximize the magnetic interaction parameter as much as possible. More details on the facility and characteristic parameters of the Stanford M-2 MHD generator can be found in references [7-9]. Details on the data acquisition instrumentation and equipment can be found in reference [14].

Cold Flow Experiments

A set of experiments using room-temperature gases in the experimental MHD channel were conducted prior to the magnetoacoustic experiments. The purpose of these cold flow experiments was to test the validity of the expression given by Eq. 7 for the reflection coefficient of the orifice, and to determine the proper value for S_R. A speaker installed in place of the M-2 combustor end plate was used as the upstream acoustic excitation source. Nitrogen was injected into the channel through the O_2 and N_2 swirl ports in the M-2 combustor. The nitrogen flow rate and the exhaust back pressure were adjusted to produce a choked flow at the downstream orifice. The Mach number in the test section was equal to about 0.11. Pressure probes located at the three locations shown in Figure 15 were used to measure the acoustic signal.

A comparison of the measured phase difference between the two upstream pressure probes and the corresponding theoretical value is shown in Figure 16. For the theoretical calculations the acoustic dissipation was computed from Eq. 6, and the best fit for the reflection coefficient was found to be 0.83, in agreement with Eq. 7 for the Mach number of 0.11. The best fit for S_R was found to be 2.6, while the geometrical value is 2.7. This difference is in agreement with the postulated error in the theory due to three-dimensional effects in the vicinity of the area change.

Excitation Source and Procedure

In the experimental MHD generator the pressure fluctation level for the background noise portion of the inherent fluctuations can be comparable to the wave-like portion, especially at low flow rates. This behavior occurs particularly at or near the transition frequencies in the phase difference, because these frequencies correspond to nodes in the acoustic part of the signals. (At a node the acoustic signal is greatly reduced, but the noise is unaffected.) The quality of the experimentally measured phase difference is greatly reduced when the background noise becomes comparable to or greater than the wave-like fluctuations. To produce good quality results, an excitation source is needed which is capable of producing acoustic-like disturbances in the MHD channel that are well above the background noise. Because the frequency spectrum of the noise is quite broad, the most effective approach is to use an excitation source that has a narrow-band frequency spectrum, and then use spectral data reduction techniques to isolate the strong acoustic-like signal from the background noise. The simplest narrow-band excitation signal is one composed of a set of discrete frequencies. In reducing the data only the results at the discrete excitation frequencies should be used, because the results at other frequencies are in general noisy and of poor quality.

To produce controlled acoustic-like disturbances in the MHD channel a voltage was applied between opposed Faraday electrodes causing a large AC current $\vec{J}'$ in the channel. The corresponding $\vec{J}' \times \vec{B}$ force on the plasma produced significant pressure fluctuations. The source of the oscillating current was a series-parallel combination of four programmable DC power supplies (Kepco model ATE 100-10M) which was capable of producing up to 200 volts and 20 amperes with a upper frequency bound of 3 kHz. The programmable source for the power supplies was a specially built sinewave synthesizer capable of producing a signal composed of up to 17 distinct sinewaves. The number of sinewaves in the signal, the frequency spacing between each sinewave, and the center frequency of the signal were all adjustable.

The values of these three parameters were selected on the basis of several physical considerations. For a fixed total power in the excitation source, the number of discrete frequencies in the signal controls the amount of power at each frequency. The more frequencies there are, the less power there is at each frequency. The maximum number of frequencies was set so that the induced acoustic-like signal in the plasma was still well above the background noise. The separation between the discrete frequencies controls the frequency resolution of the measurements. The bandwidth of the signal is equal to the number of discrete frequencies times the frequency separation. A larger bandwidth means fewer separate center frequencies are needed to cover the entire frequency range of interest. A trade-off exists between higher resolution and larger bandwidth. To reduce the effects of possible drifts in the experimental conditions, it is desirable to keep the number of center frequencies small,

and thereby keep the duration of the time required to acquire the data small. Most of the data were acquired with either a one or two Hertz frequency resolution and with five discrete frequencies used for each center frequency.

EXPERIMENTAL RESULTS AND DISCUSSION

Results

Proper performance of the excitation source was critical to the success of the magnetoacoustic experiments. A typical power spectral density plot for the signal measured by the upstream pressure probe is shown in Figure 17. The excitation frequencies for this case were centered around 155 Hz. These results show that the pressure signal produced by the source contains the desired narrow peaks at the discrete excitation frequencies, and that the signals for the excitation frequencies are significantly above the background noise.

The introduction of a pressure oscillation in the plasma at a given frequency does not guarantee that the disturbance will be wave-like. The coherence (a measure of the portion of energy in one signal, which is correlated to the energy in the other signal [15]) measured by two pressure probes at different locations in the channel can be employed to determine the extent to which the excited disturbance is propagational in character. A wave-like fluctuation produces a coherence of 1.0, while a noise fluctuation produces a low coherence of 0.2 or less. A typical coherence plot is shown in Figure 18 for the same conditions as Figure 17. The coherence is near one at low frequencies and drops off near the frequency at which the first node is located at the upstream pressure probe. The background coherence rises again after the frequency at which the first node passes the downstream pressure probe. The narrow peaks in the coherence around 155 Hz demonstrate that the excitation source is producing a strong wave-like disturbance that is spectrally well above the background noise.

The excitation frequencies were incremented to cover the range of frequencies from 120 Hz to 260 Hz which spans the range of the first transition as shown in Figure 13. At each excitation frequency the phase difference between the upstream and the downstream pressure probes determined for the cases of ordinary acoustics and of magnetoacoustics is shown in Figures 19 and 20, respectively. Included in these figures is the corresponding theoretical value computed using the two region model and the MHD dispersion relationship. The experimental MHD conditions are identical to those depicted in Figures 1-3.

Discussion

The data in Figures 19 and 20 represent preliminary results obtained from the most recent set of magnetoacoustic experiments performed at Stanford. The experimental data and the theory are seen to be in very good agreement. The data in both figures appear to fall slightly inside and below the theoretical curves. This behavior is also observed in the cold flow data in Figure 16 and indicates that the difference is due to the acoustic model and not to any MHD effects. The change in the phase difference dependence on frequency is quite noticable between the two conditions shown separately in Figures 19 and 20. The peak value of the phase difference is reduced from 110 degrees in the normal acoustic case to 85 degrees in the magnetoacoustic case. The

differences between the two figures are mostly due to an increase in k_i of about 0.13 for the magnetoacoustic waves, in comparison with a value of about 0.03 for the normal acoustic waves. The predicted changes in the phase velocities are relatively small (less than 5 percent in the measured range of frequencies) and could not be determined from the present data owing to the scatter shown in Figure 20. The relatively large Faraday load factor was responsible for the small effect on the phase velocities. The external load resistor used in the experiments was only 0.7 ohms, but the large boundary layer resistances were responsible for the high value of the effective Faraday load factor.

Future work will concentrate on refining the data reduction procedures employed for the present measurements, and on analyzing additional data to examine the consistency of the model. The present results may be improved by accounting for small variations on the experimental conditions (particularly the current density), that occurred during the time required to measure the phase difference over the entire frequency range. An analysis of additional data acquired during these experiments will be used to test the consistency of the model by comparing the phase difference between different pairs of pressure probes measured at the same time, and by comparing phase differences between the same pressure probes measured under different MHD conditions. The latter analysis will be particularly important in determining the effect of the magnetic interaction parameter on the damping factor k_i.

CONCLUSIONS

Interactions between the magnetoacoustic fields and the electrical power circuitry can have detrimental effects on the performance of an MHD generator. Previous theoretical studies of these interactions have been based primarily on examining the solutions of an MHD dispersion relationship. The derivation of this relationship contains many assumptions and approximations whose validity has never been successfully tested experimentally. The magnitude of the magnetoacoustic effects in laboratory-scale MHD generators is small, but experiments to compare with the theory can be performed by making measurements at low frequencies where the predicted effects are the largest.

A simple acoustic model of the experimental MHD generator has been developed and used in conjunction with the MHD dispersion relations to predict the pressure field in the MHD generator. An experimental approach using the phase difference between pressure signals measured at different locations in the MHD channel to detect small MHD effects on both the damping and the phase velocity of magnetoacoustic waves has been developed and has proven to be quite sensitive to small changes. To make these measurements, propagating low frequency pressure fluctuations in an MHD channel were excited using a specially designed external power source to produce oscillations in the current between a pair of opposed electrodes located upstream of the MHD channel. A preliminary analysis of the data shows good agreement between the measured and predicted MHD effect of wave amplitude damping on the phase difference. The predicted changes in the phase velocities of the waves were too small to detect owing to the scatter in the data. Work is in progress to improve the data reduction procedure employed with the present data, and to examine additional data taken under different operating conditions. The measurements reported here are believed to be the first to provide experimental support for the predicted MHD effects on acoustic waves.

ACKNOWLEDGEMENTS

This work was supported by the National Science Foundation under grant NSF CPE 82 17622, and by the U. S. Department of Energy under contract no. DE-AC01-80ET15611.

REFERENCES

1. Velikov, E. P., "Hall Instability of Current-Carrying Slightly-Ionized Plasmas", Symp. MHD Electrical Power Generation, Newcastle-upon-Tyne, G.B., 135, (1962).

2. Wright, J. K., "A Temperature Instability in MHD Flow", Proc. Phys. Soc. 81, 498, (1963).

3. McCune, J. E., "Wave Growth and Instabilities in Partially-Ionized Gases", Intl. Symp. on MHD Electrical Power Generation, Paris, Paper 33, (1964).

4. Locke, E. V., and J. E. McCune, "Growth Rates for Axial Magneto-Acoustic Waves in a Hall Generator", AIAA Journal 4, 1748, (Oct. 1966).

5. Powers, W. L., and J. B. Dicks, "Transient Wave Growth in MHD Generators", AIAA Journal 6, 1007, (June 1968).

6. Fishman, F. J., "Instabilities of Hall MHD Generators to Magneto-Acoustic Waves", AVCO-Everett Research Lab Report 323, (Feb. 1969).

7. Barton, J. P., "Fluctuations in Combustion-Driven MHD Generators", HTGL Report No. 118, Stanford University, August 1980.

8. Koester, J. K. et al, "Integrated MHD Generator-Inverter System Test Results at CDIF", Twenty-first Symp. on Engineering Aspects of MHD, Argonne, IL, (1983).

9. Simons, T. D., "Acoustic and Entropy Waves in a Combustion MHD Generator", HTGL Report No. 203, Stanford University, June 1982.

10. Simons, T. D., R. H. Eustis, and M. Mitchner, "Measurements of Propagating Acoustic and Entropy Waves in a Combustion MHD Generator", Twentieth Symp. on Engineering Aspects of MHD, Irvine, CA, (1982).

11. Walker, J. S., "Long Wave Length Analysis For Fluctuations in Plasma MHD Generators", Twentieth Symp. on Engineering Aspects of MHD, Irvine, CA, (1982).

12. Temkin, S., Elements of Acoustics, John Wiley & Sons, New York, (1981).

13. Davis, S., "Transmission of Sound from a Nozzle Carrying a Compressible Subsonic Flow"' Paper presented at the 86th meeting of the Acoustical Society of America, Los Angeles, (Oct. 30 - Nov. 2, 1973.)

14. Munce, Jr., A. C., M. Mitchner, and J. K. Koester, "Magnetoacoustic Effects on Phase Velocity of Waves in MHD Generators", Twenty-first Symp. on Engineering Aspects of MHD, Argonne, IL, (1983).

15. Bendat, J. S., and A. G. Piersol, Random Data: Analysis and Measurement Procedures, Wiley-Interscience, New York, (1971).

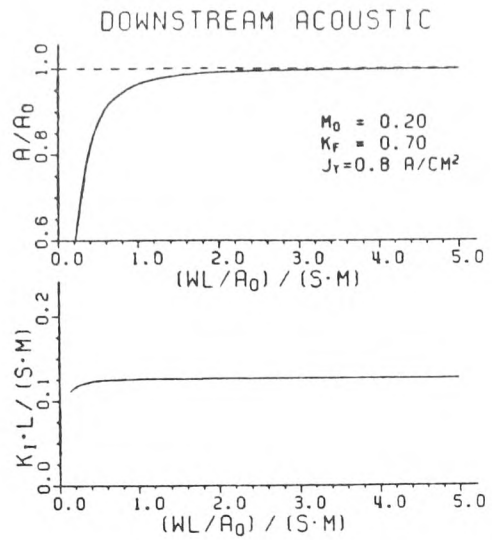

Figure 1. Results of MHD dispersion relationship for effects on (a) Phase Velocity, and (b) Damping Coefficient of the downstream-traveling magnetoacoustic wave.

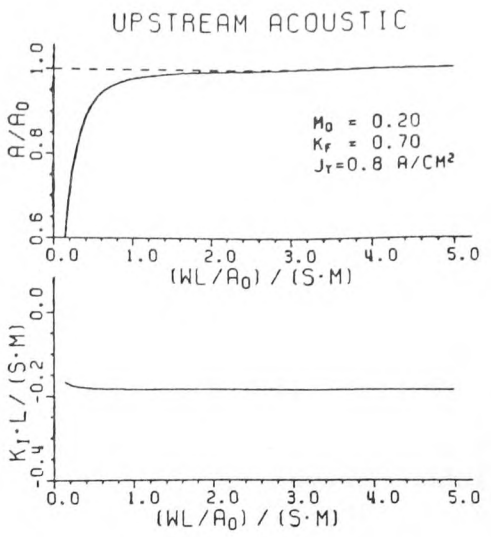

Figure 2. Results of MHD dispersion relationship for effects on (a) Phase Velocity, and (b) Damping Coefficient of the upstream-traveling magnetoacoustic wave.

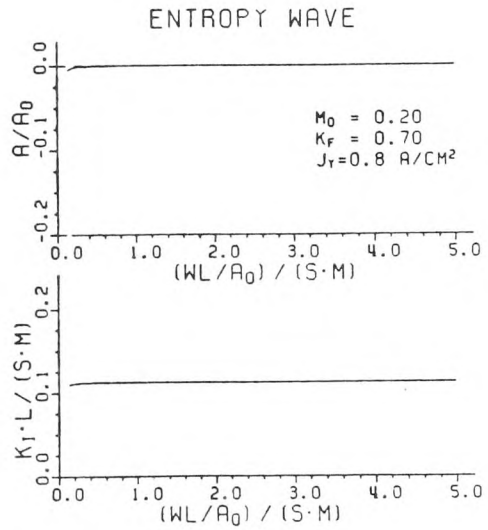

Figure 3. Results of MHD dispersion relationship for effects on (a) Phase Velocity, and (b) Damping Coefficient of the magnetoentropic wave.

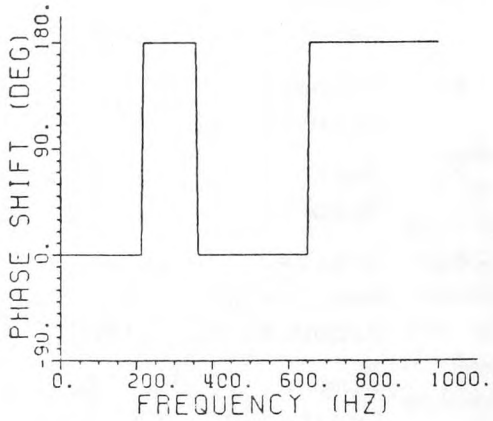

Figure 5. Phase Difference between pressure signals at two different channel locations versus Frequency (for the ideal conditions M=0, R_1=1, and k_i=0).

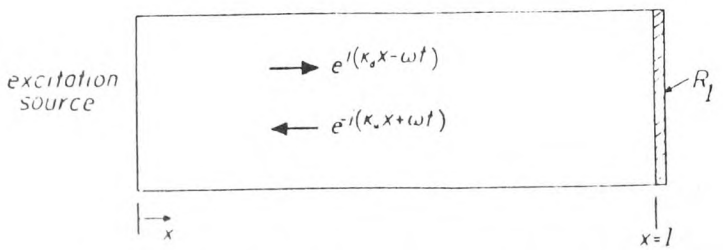

Figure 4. Schematic of the simplest acoustic model for an MHD generator.

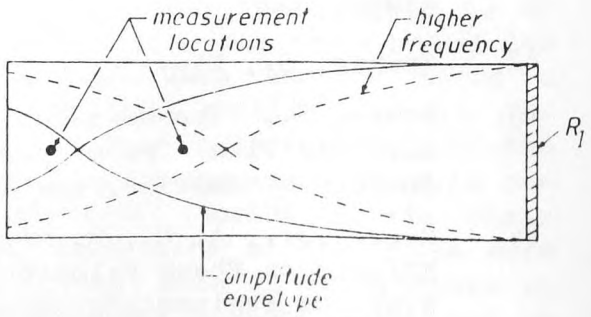

Figure 6. Envelope of the standing-wave pressure fluctuations for two different frequencies (closed end boundary condition).

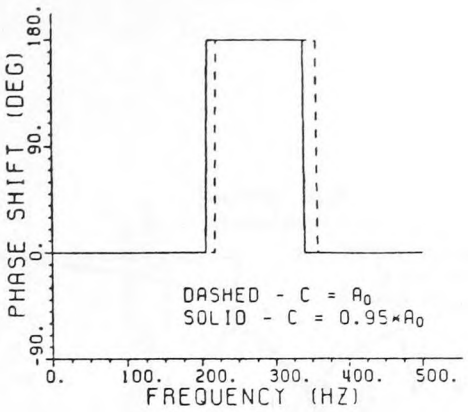

Figure 7. Effect on the Phase Difference due to a 5 percent change in the Average Phase Velocity.

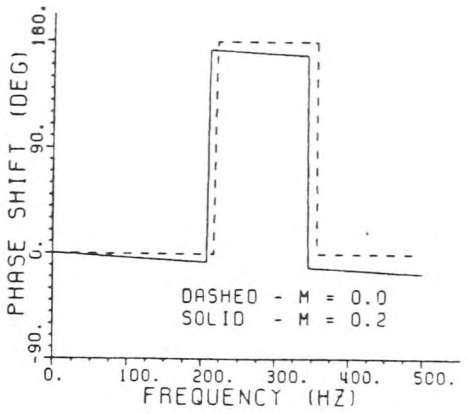

Figure 8. Effect on the Phase Difference due to a Mean Flow Velocity (Mach number = 0.2).

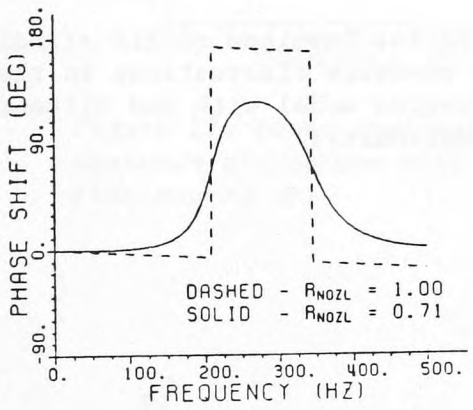

Figure 9. Effect on the Phase Difference due to an imperfectly Reflecting Downstream Boundary Condition (R_1 = 0.71).

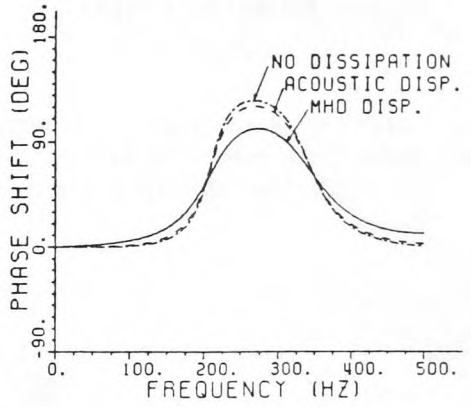

Figure 10. Effect on the Phase Difference due to Dissipation, (1) no dissipation, (2) normal acoustic dissipation, and (3) MHD dissipation.

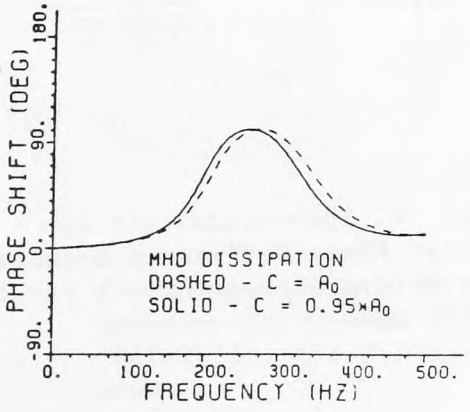

Figure 11. Combined effect on the Phase Difference of Dissipation and a 5 percent change in the Average Phase Velocity.

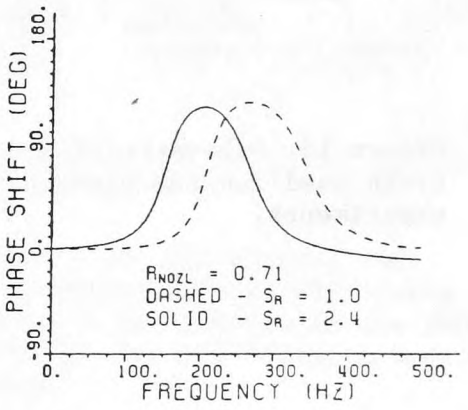

Figure 13. Effect on the Phase Difference due to an Area Change (from 1.0 to 2.4).

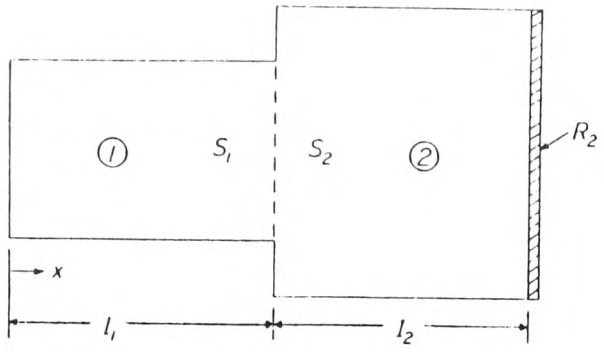

Figure 12. Schematic of the Two Region Acoustic Model.

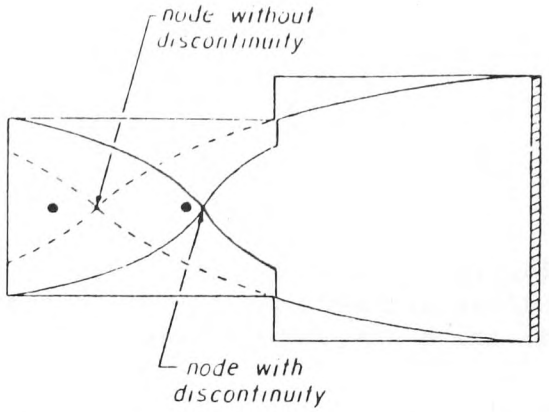

Figure 14. Envelope of the standing-wave pressure fluctuations in the two region model with and without a discontinuity.

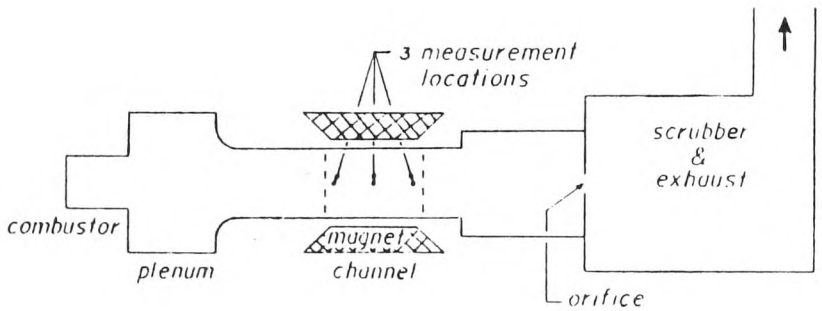

Figure 15. Schematic of M-2 flow-train used for the magnetoacoustic experiments.

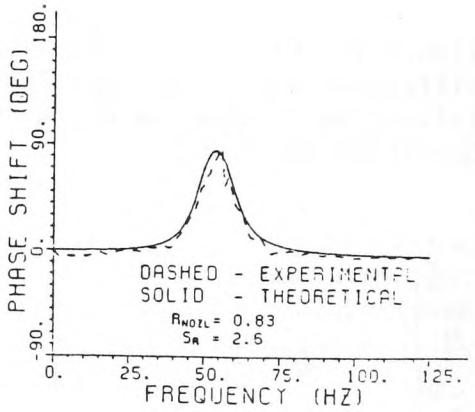

Figure 16. Theoretical fit to Measured Phase Difference between two upstream microphones in the cold N_2 flow case.

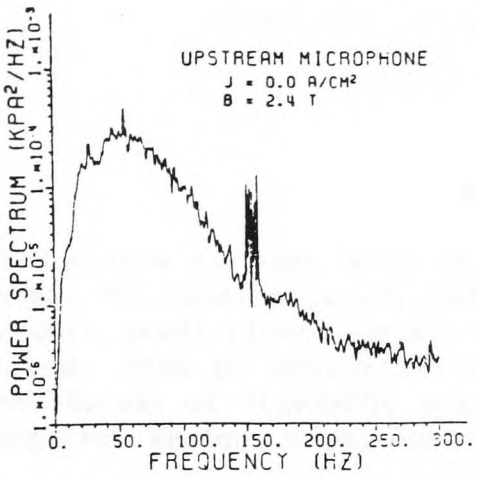

Figure 17. Power Spectral Density of upstream microphone with the excitation source on.

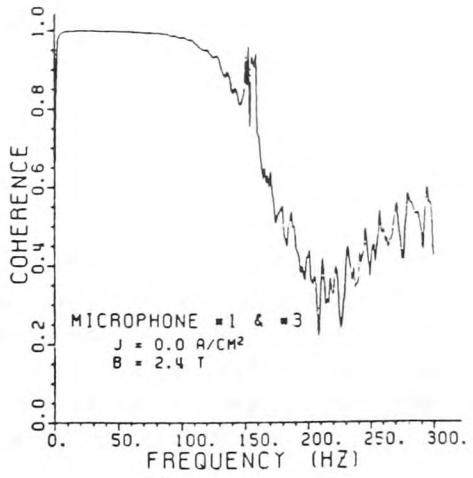

Figure 18. Coherence between microphones for the case when the excitation source was on.

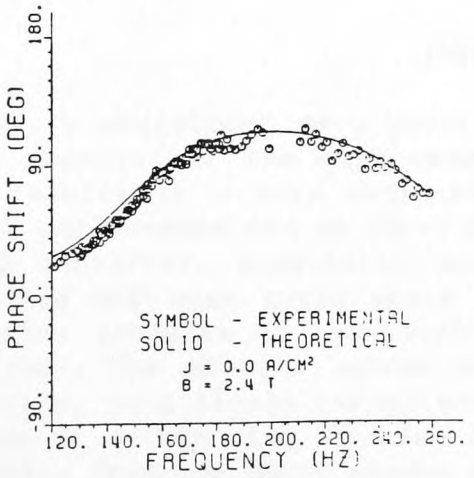

Figure 19. Theoretical and Experimental Phase Difference between microphones in the MHD channel for the Ordinary Acoustics case.

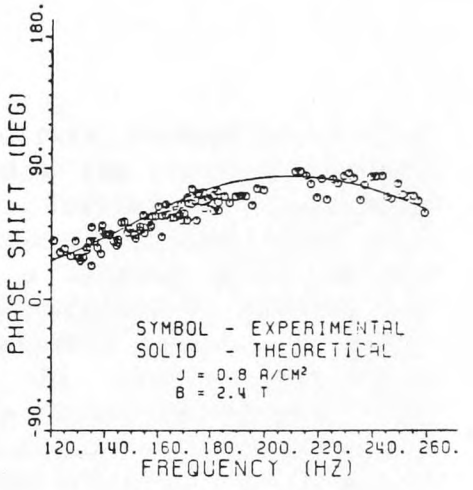

Figure 20. Theoretical and Experimental Phase Difference between microphones in the MHD channel for the Magnetoacoustics case.